Microstructure and mechanical properties of a rare earth rich magnesium casting alloy

V. Angelini, I. Boromei , L. Ceschini, A. Morri

This research activity was focused on the microstructural and mechanical characterization of an innovative rare earth rich magnesium alloy, EV31A (Elektron 21®), in the sand cast and standard T6 conditions. Microstructural analyses were carried out by means of optical and scanning electron microscopy, in order to highlight the microstructural evolution induced by the heat treatment. The results show different intermetallic particles and eutectic compounds which, depending on their composition, may dissolve or not during solution treatment.
Specific yield and ultimate strength of the investigated alloy were reported to be higher if compared to the more common AZ91 magnesium alloys and comparable to that of the widely used A356 cast aluminum alloy.

KEYWORDS: MAGNESIUM ALLOY - HEAT TREATMENT - MICROSTRUCTURE - MECHANICAL PROPERTIES

INTRODUCTION

Recent studies highlighted that some rare earth (RE) metals, such as Yttrium (Y), Neodimium (Nd), Gadolinium (Gd) are very effective elements to improve the mechanical properties of Mg alloys, along with their corrosion resistance [1-3]. Mg alloys are very attractive for several industrial applications, in particular in the aerospace and automotive fields thanks to their lightness, high specific strength, high damping capability and good castability, [4]. The magnesium alloy analyzed in the present investigation is the innovative alloy EV31A, with neodymium and gadolinium as main alloying elements, respectively up to 3.1wt% and 1.7wt%. Zirconium is also present because of the relevant grain refinement potential of Zr-rich primary particles, as a results of its peritectic transformation, and its amount is close to the maximum solubility of Zr in molten magnesium (0.6 wt. %). Zn enhances the mechanical properties, due to the precipitation hardening effect; furthermore, it helps to overcome the corrosive effects of Fe and Ni impurities [5].

The high content of rare earth allows achieving good mechanical properties via precipitation hardening. The alloy investigated in the present study is mainly used in military and aerospace fields. The main transmission housing of Boeing AH-64D Apache and the power transfer module (PTM) of Expeditionary Fighting Vehicle (EFV) are relevant examples [6]. The standard heat treatment for EV31A magnesium alloys, suggested by the supplier, consists of solubilization at 520 °C for 8 h, followed by hot water quench (60-70 °C) and aging at 200 °C for 16 h [5]. The aim of the present study was to investigate the effect of heat treatment on microstructure and, consequently, on the hardness and tensile properties of this sand-cast magnesium alloy.

EXPERIMENTAL

The alloy studied in the present work was provided by Magnesium Elektron®, as sand-cast plates (200mm x 200mm x 25mm), with the chemical composition reported in Table 1.

Nd	Gd	Zr	Zn	Fe	Ni	Cu	Si	Ag	ORE	Mg
2.8	1.3	0.56	0.29	0.003	<0.0010	<0.008	<0.01	<0.1	0.14	Balance

Tab. 1 - Chemical composition of EV31A (wt.%), ORE=other rare earths.
Composizione chimica della lega EV31A (wt.%).

V. Angelini, I. Boromei, L. Ceschini, A. Morri
Department of Industrial Engineering (DIN),
Alma Mater Studiorum
University of Bologna, V.le Risorgimento 4,
40136 Bologna

SF_6 cover gas was used to prevent burning during the melting process. Different samples were cut from the sand cast plates and heat treated in an electrical resistance furnace. According to the heat treatment parameters suggested by the supplier, the samples were subjected to solution treatment at 520 °C for 8h, subsequently quenched in hot water at 70 °C and finally artificially aged at 200 °C for 16 h. Temperature fluctuations were limited to ± 2° C, during the solution treatment, and ± 1 °C during the final aging treatment. The microstructure of the

alloy, in the as-cast condition and after heat treatment, was analyzed by optical (OM) and scanning electron microscopy (SEM), equipped with an Energy Dispersive Spectroscopy (EDS) microprobe. Microstructural characterization was carried out on samples prepared by standard metallographic techniques and etched with HNO_3 2 vol.% in ethanol (Nital 2), or 5 mL acetic acid, 6g picric acid, 10 mL water and 100 mL ethanol (Acetic Picral). Deep etching with HNO_3 20 vol.% - EtOH 80 vol.% was also used to highlight some precipitates at grain interiors. Image analyses on the optical micrographs (OM) were carried out using the ®Image Pro-Plus software. Grain size was evaluated using the linear intercept method, according to ASTM E112-10 [7]. Brinell hardness tests were performed according to ISO 6506-1 standard [8], using a 62.5 kg load and a 2.5 mm steel ball as indenter. Tensile tests were also performed according to ISO 6892-2 standard [9], using flat specimens with a 36 mm gauge length, 10 mm gauge width and 4 mm in thickness. Fracture surfaces of tensile specimens were analysed by SEM-EDS to study the mechanisms of failure.

RESULTS AND DISCUSSION

Microstructural analysis of the sand cast alloy

Optical micrograph of the sand cast alloy etched with Nital 2 and SEM magnification, with corresponding EDS analysis, are reported in Fig.1 (a-b). The microstructure consists of equiaxed grains with an average grain size of 45 ± 2 μm, surrounded by the eutectic compound, indicated by the arrows. SEM-EDS analyses of the eutectic highlighted that it is composed by α-Mg and Mg-Nd-Gd ternary phase.

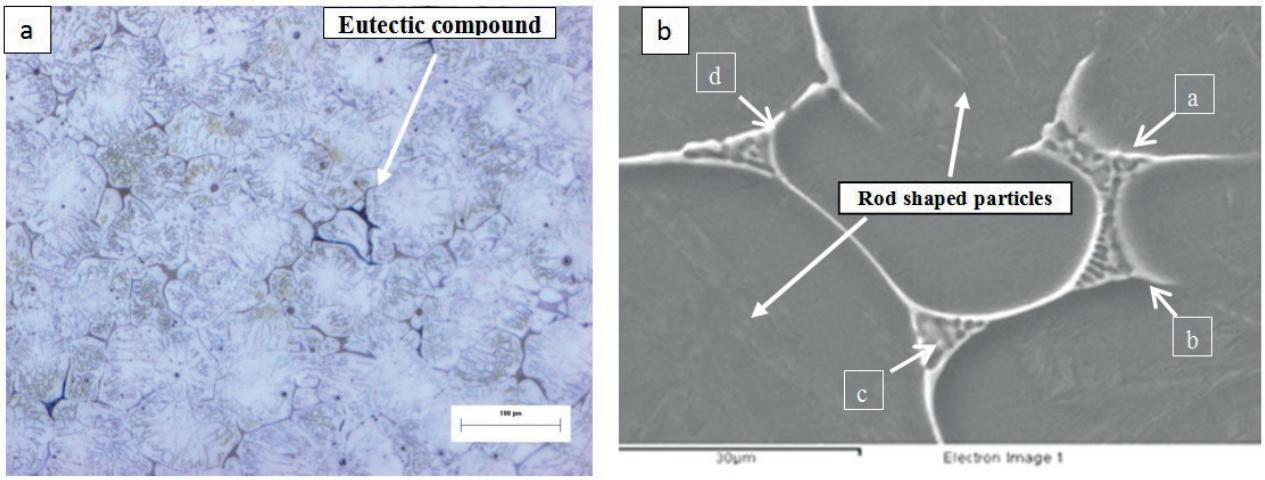

	Mg (at.%)	Nd (at.%)	Gd (at.%)	Zn (at.%)	O (at.%)	Mg at.% / Nd at.% + Gd at.%
Spectrum a	86.93	6.15	0.95	1.44	4.53	12.24
Spectrum b	85.96	5.88	0.90	1.70	5.56	12.67
Spectrum c	89.54	6.05	0.81	1.44	2.17	13.01
Spectrum d	86.71	6.22	0.95	1.76	4.35	12.09

Fig. 1 - Optical (a) and SEM (b) micrographs, with corresponding EDS analyses, of the eutectic compound in the as-cast alloy.
Micrografia ottica (a) e immagine SEM con analisi EDS del composto eutettico nella lega dopo solidificazione.

The atomic ratio between Mg and Nd + Gd in the eutectic is between 12 and 13, very close to the stoichiometric ratio, equal to 12. It can be therefore assumed that this phase is the $Mg_{12}(Nd_x;Gd_{1-x})$, a modification of the metastable phase $Mg_{12}Nd$, where neodymium is substituted by gadolinium without changing the crystal structure. In fact, Nd and Gd show small differences between the atomic radii, (r_{Gd}=0.1802 nm, r_{Nd}= 0.1821 nm). The SEM micrograph in Fig.1-b also evidences the presence of rod-shaped particles, of sub-micrometric and micrometric size inside the grains, but they were not clearly visible by SEM on the metallographic samples etched by Nital2. SEM-EDS line profiles of the main elements, across a grain, are reported in Fig. 2, highlighting the presence of Zr clusters inside the grains, not revealed by the OM and SEM images in Fig.1 obtained on samples etched with Nital 2.

SEM images of the sand cast sample, after deep etching with 20% HNO_3 - 80% EtOH, is shown in Fig. 3. This etching allows to highlight the presence of some intermetallic compounds inside the grains (Fig. 3-a) and Zr cluster at the grain centre (Fig. 3-b). The SEM-EDS analyses reported in Fig. 4 shows that the thin precipitates are mainly composed by Neodymium and Gadolinium. Due to their small size, however, it was not possible to determine their stoichiometric composition.

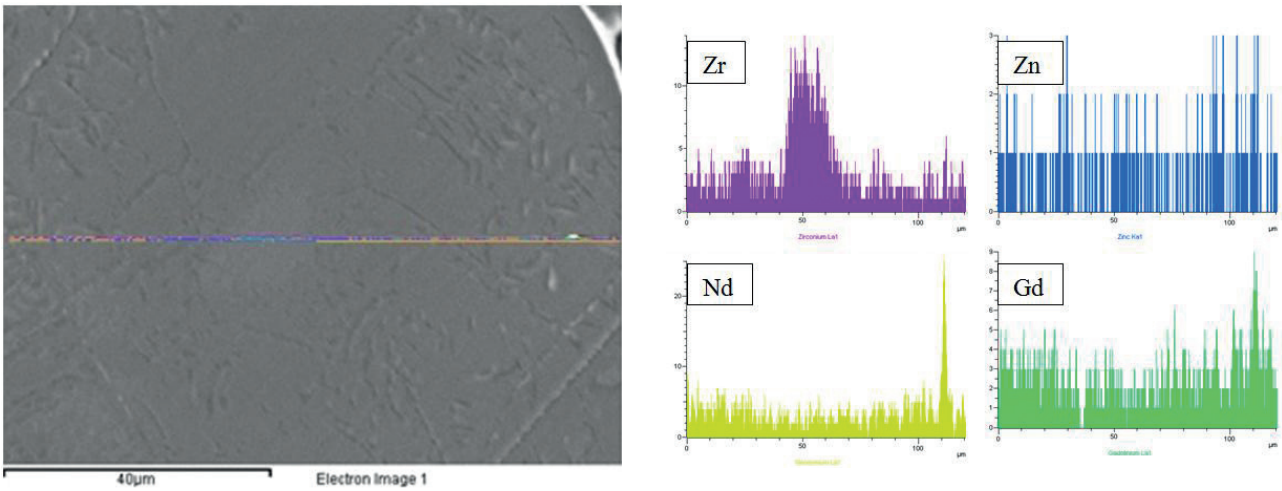

Fig. 2 - SEM micrograph with corresponding element line profiles across a grain in the as-cast alloy.
Immagine SEM con profili EDS di linea rilevati lungo un grano.

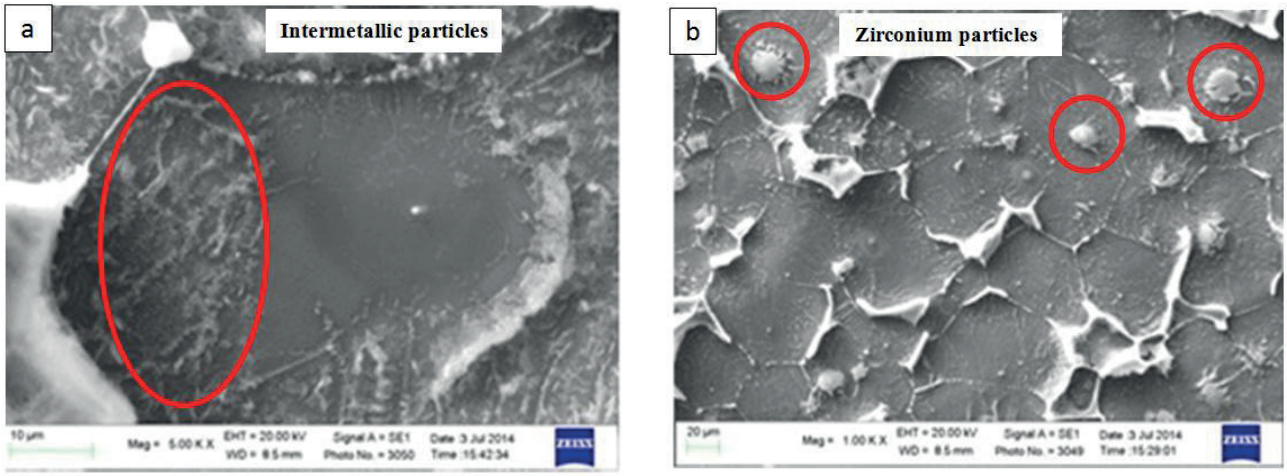

Fig. 3 - SEM micrographs of the as cast alloy after deep etching with 20% HNO_3-80% EtOH:
(a) intermetallic particles; (b) Zr clusters inside the grains.
Immagini SEM della lega dopo solidificazione dopo attacco profondo con 20% HNO_3-80% EtOH:
(a) composti intermetallici; (b) addensamenti di Zr nei grani.

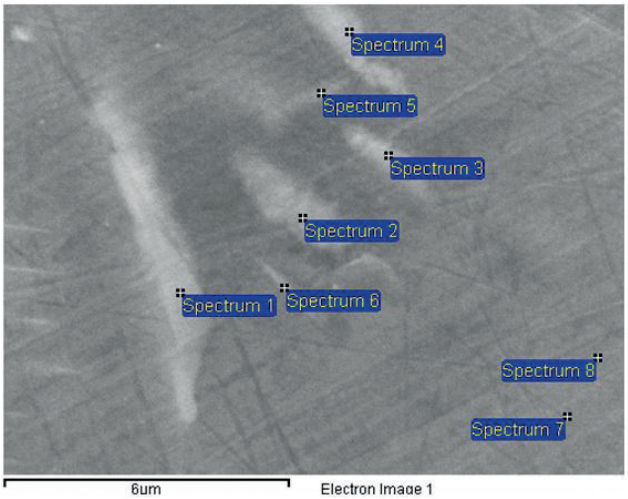

	Mg [wt.%]	Nd [wt.%]	Gd [wt.%]	Zn [wt.%]	Zr [wt.%]
Spect. 1	88.30	8.61	1.81	0.54	0.74
Spect. 2	89.65	6.32	2.02	1.21	0.80
Spect. 3	95.89	1.45	1.24	0.26	1.15
Spect. 4	95.43	2.11	1.15	0.35	0.95
Spect. 5	94.85	2.30	1.42	0.23	1.21
Spect. 6	96.58	1.35	0.82	0.27	0.99
Spect. 7	95.44	1.74	0.57	0.35	1.90
Spect. 8	94.78	1.79	1.80	0.26	1.36

Fig. 4 - SEM-EDS micrograph with corresponding EDS analysis of intermetallic particles on the as-cast alloy.
Micrografia SEM con analisi EDS dei composti intermetallici presenti nella lega dopo solidificazione.

Microstructure of the T6 heat-treated alloy

Optical micrographs at different magnification of the T6 heat-treated alloy are reported in Fig 5. The microstructural evolution induced by standard T6 heat treatment can be appreciated by comparing representative optical micrographs of the sand-cast (Fig.1) and heat-treated alloy (Fig.5).

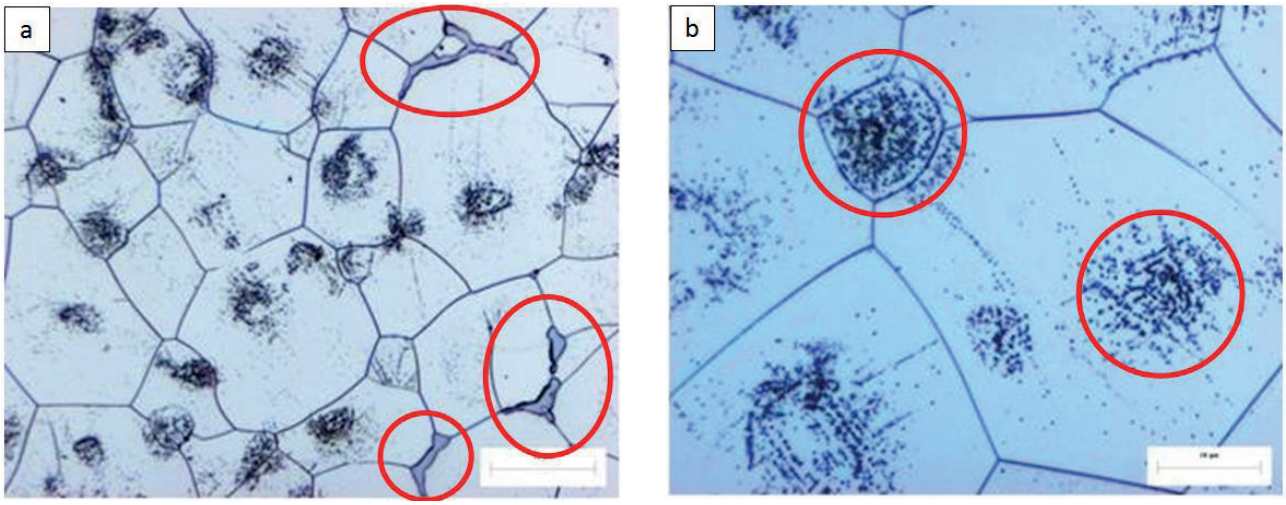

Fig. 5 - Optical images of the alloy in T6 condition etched with Nital2: eutectic compound (a) and Zr-Zn clusters (b).
Immagini in microscopia ottica della lega trattata T6 attacata con Nital2: (a) composto eutettico; (b) addensamenti Zr-Zn.

From Fig. 5-a it can be clearly seen that the eutectic compound $Mg_{12}(Nd_x;Gd_{1-x})$ (highlighted by red circles), did not completely dissolve during the solution treatment, while the intragranular intermetallic precipitates shown in Fig 3-a are no longer visible. Moreover, the presence of particles inside the grains (indicated in the red circle) is clearly visible in Fig. 5b; they aggregated as clusters and react with Nital2. SEM-EDS analyses on these clusters showed that are mainly based on Zr-Zn, due to Zn diffusion during solutioning, as confirmed by the EDS analyses reported in Fig. 6 (spectra 3 to 5).

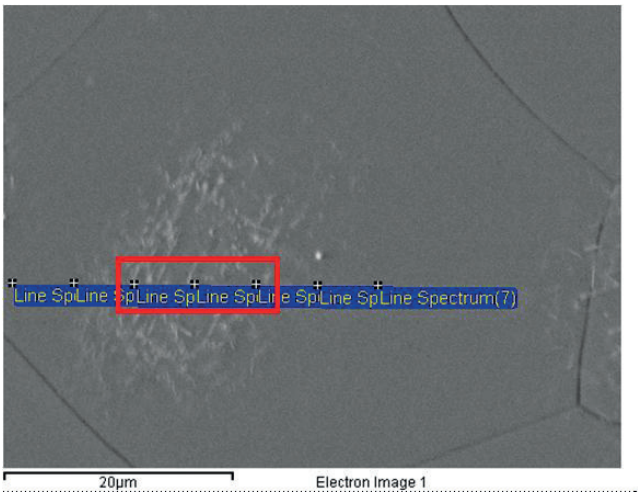

	Mg [at.%]	Nd [at.%]	Gd [at.%]	Zn [at.%]	Zr [at.%]
Spect. 1	99.34	0.50	0.17	0.00	0.00
Spect. 2	98.98	0.47	0.21	0.00	0.34
Spect. 3	96.94	0.49	0.17	0.68	1.72
Spect. 4	96.21	0.47	0.00	0.35	2.97
Spect. 5	97.04	0.44	0.00	0.73	1.79
Spect. 6	98.90	0.53	0.23	0.00	0.33
Spect. 7	99.37	0.48	0.14	0.00	0.00

Fig. 6 - SEM image and EDS results (at. %) on the Zr-Zn clusters in the T6 heat treated alloy
Immagine SEM e corrispondente analisi EDS sugli addensamenti a base Zr-Zn

The strength of this Mg-RE alloy is achieved via precipitation hardening, induced by the T6 heat treatment, which involves solutioning, quenching and artificial aging. As reported in [10], the precipitation sequence, from the supersaturated solid solution involves the formation of multiple phases designated as β^{II} (Mg_3RE with $D0_{19}$ crystal structure), β^{I} ($Mg_{12}RE_2$ with base centered orthorhombic crystal structure) and β, that has the same chemical composition (Mg_3RE) of the β^{II} phases, but precipitates with a $D0_3$ (face centered cubic, FCC) crystal structure. Further characterization on these phases by TEM are currently under investigations by the authors.

Hardness and tensile properties

Results of Brinell hardness and tensile tests for the sand cast and T6 heat-treated EV31A (Elektron 21®) alloy are reported in Table 2. The yield strength (160MPa) and the ultimate tensile strength

(260 MPa) are higher when compared to other, more common magnesium alloys, such as the AZ91 alloy (YS=120 MPa; UTS=200 MPa) [11]. Moreover, it is worth noting that the tensile properties, in terms of specific strength (shown in Fig.7-a), are comparable to those of the most widely used A356 (G-AlSi7Mg) alloy in T6 condition [12].

Sample	HB 10	YS [MPa]	UTS [MPa]	E%
1	76	160.5	240	2.5
2	75	159.5	264	4.3
3	78	159.0	265	4.3
4	76	162.0	267	4.9
Average	76.5	160	259	4.00
Dev.st.	1.2	1.3	12.5	1.0

Tab. 2 - Tensile properties and Brinell hardness of the sand cast and T6 heat treated EV31A magnesium alloy.
Proprietà a trazione e durezza della lega di magnesio EV31A colata in sabbia e trattata T6.

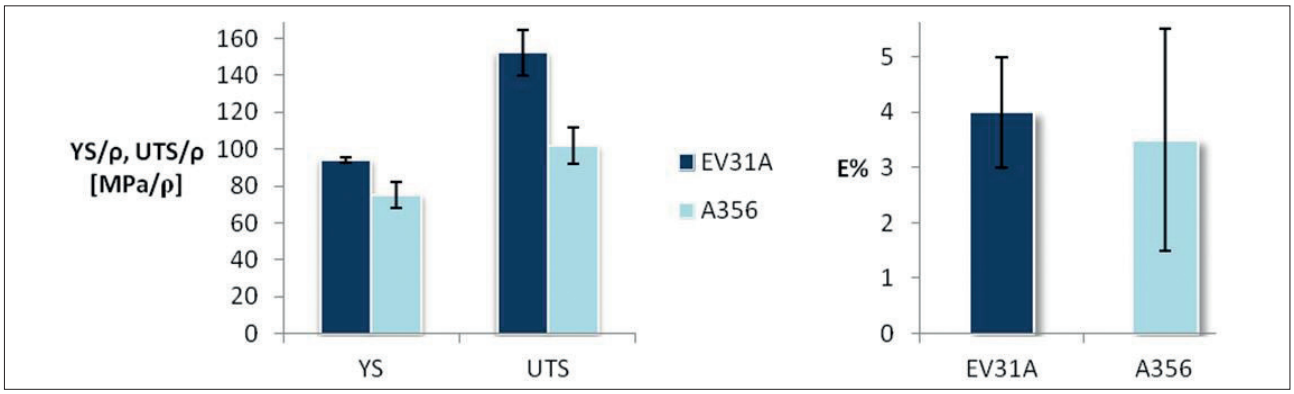

Fig. 7 - Comparison of the specific tensile properties of magnesium alloy EV31A and aluminium alloy A356 , both T6 heat treated.
Confronto delle proprietà tensili specifiche della lega EV31A con la lega A356 entrambe dopo trattamento termico T6.

Fracture surfaces

SEM analyses of the fracture surfaces of the T6 heat-treated alloy highlighted the eutectic compound still present at the grain boundaries (Fig. 8-a). Different failure mechanisms can be appreciated: fracture of the eutectic compounds (Fig. 8-b), cleavage planes (Fig. 8-c), decohesion at the grain boundaries and few regions with small dimples (Fig. 8-d). The presence of large eutectics regions favour nucleation of microcracks, that propagate both along grain boundaries and across the grains, leading to cleavage fracture. The fracture surfaces, in fact, show a transgranular and intergranular mixed fracture mode. Moreover, fractographic analyses did not highlight casting defect, such as porosities or oxides.

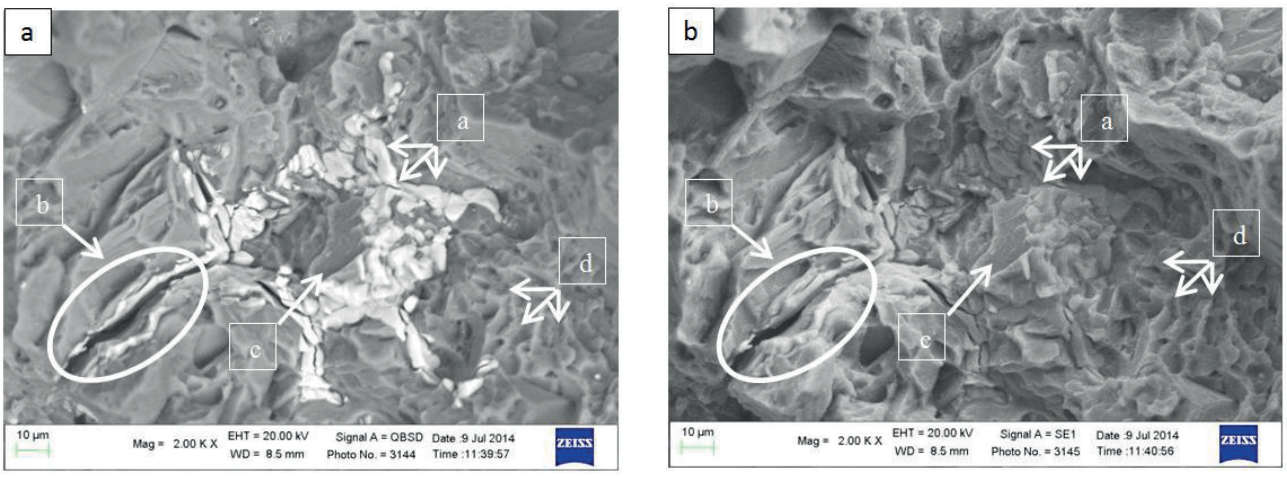

Fig. 8 - SEM images of fracture surface obtained by back scattered (a) and secondary (b) electrons.
Immagine SEM delle superfici di frattura ottenute tramite elettroni retrodiffusi (a) ed elettroni secondari (b).

CONCLUSIONS

In the present work, the microstructural evolution due to T6 heat-treatment in the sand-cast magnesium alloy EV31A was investigated. This innovative Mg alloy is characterized by high total content of rare earth elements (Nd and Gd) up to about 4 wt.%.

The as-cast alloy presented equiaxed grains, surrounded by ternary eutectic compound $Mg_{12}(Nd_x;Gd_{1-x})$; intermetallic phases, based on Nd and Gd, were also observed. SEM-EDS analyses, after deep etching, also allowed identifying Zr clusters at grain interior.

Remarkable microstructural changes, that can be appreciated by OM and SEM analyses, characterized the T6 heat-treated alloy, with respect to the sand-cast one. The solution treatment, favoring Zn diffusion, led to the formation of clusters of Zr-Zn rod-shaped precipitates at the grain centre, and dissolved the Nd-Gd intermetallic precipitates, but it was not able to completely dissolve the eutectic compound at the grain boundaries. The tensile tests showed high specific strength of the T6 heat-treated alloy and good ductility (with values comparable to those of the A356 Al-Si-Mg alloy), in spite of the brittle morphology present on the fracture surface.

REFERENCES

[1] Smola B, Stulı I, von Buch F, Mordike BL. Structural aspects of high performance Mg alloys design. Mater Sci Eng A 2002;324:113-7.

[2] Wu G, Fan Y, Gao H, Zhai C, Zhu YP. The effect of Ca and rare earth elements on the microstructure, mechanical properties and corrosion behavior of AZ91D. Mater Sci Eng A 2005;408:255-63.

[3] E.D. Morales, E. Ghali, N. Hort, W. Dietzel, K.U. Kainer MS, 419-422 F. Corrosion behaviour of magnesium alloys with RE additions in sodium chloride solutions. Mater Sci Forum 2003;419-422:867-72.

[4] Mordike BL, Ebert T. Magnesium Properties - applications - potential. Mater Sci Eng A 2001;302:37-45.

[5] Nie J-F. Precipitation and Hardening in Magnesium Alloys. Metall Mater Trans A 2012;43:3891-939.

[6] Luo A a. Magnesium casting technology for structural applications. J Magnes Alloy 2013;1:2-22.

[7] Astm E112-10 - Standard Test Methods for Determining Average Grain Size 2012:1-27.

[8] International Organization for Standardization. ISO 6506-1 2014.

[9] International Organization for Standardization. ISO 6892-2 2013.

[10] Honma T, Ohkubo T, Hono K, Kamado S. Chemistry of nanoscale precipitates in Mg-2.1Gd-0.6Y-0.2Zr (at.%) alloy investigated by the atom probe technique. Mater Sci Eng A 2005;395:301-6.

[11] Elektron M. Magnesium Casting Alloys - Datasheet 440. 2006.

[12] Ceschini L, Morri A, Morri A. Effects of the Delay Between Quenching and Aging on Hardness and Tensile Properties of A356 Aluminum Alloy. J Mater Eng Perform 2012;22:200-5.